

4 X-ray diffraction techniques

4.1 Introduction

An integral part of the process of crystal structure determination is an experiment and the techniques used to collect the experimental data. The experiment consists of scattering radiation from crystalline matter, the radiations that are usually employed being X-rays, electrons and neutrons. Although all three radiations can be employed, the vast majority of structure determinations are based on X-ray diffraction data. This chapter will therefore be dedicated to X-ray techniques. It is, however, important to point out that all the other chapters are applicable to all three diffraction techniques. We begin this chapter by introducing the Laue and Bragg conditions, and their geometrical representation in terms of the Ewald sphere of reflection. These conditions are common to all the experimental techniques that will be discussed. We shall next discuss in some detail the principles of operation of traditional and modern sources of X-rays: the X-ray tube and its spectroscopic fundamentals, and the vastly more powerful synchrotron. Our discussion of sources of X-radiation will be followed by an outline of the operation of some area detectors for this radiation: (i) photographic film, which may be thought to have become of historical importance only but which has lasting underlying principles; (ii) the imaging plate, which is geometrically analogous to X-ray film but has different physical principles and greatly enhanced performance; and (iii) the charge-coupled device, which produces very efficiently a digital image of the diffraction pattern. We shall next discuss the instrumentation which is employed with the above sources and detectors for the generation of diffraction patterns. The rotation method will be treated in some detail, the principles of the Weissenberg, de Jong–Bouman and precession methods will be briefly indicated, and a detailed discussion of the four-circle diffractometer will be presented. The four-circle diffractometer is a very precise device, which enables one to measure very accurately one reflection at a time and uses a photon counter as a detector. The chapter is concluded with a discussion of the Laue method. This was the first method ever employed in the production of diffraction patterns, it had limited application, and was for a long time considered to be mainly of historical interest. However, with the advent of synchrotrons and highly linear and fast detectors, the Laue method has seen a major revival and is nowadays being applied to collect extensive amounts of data. We shall see how, in principle, a Laue pattern can be calculated—which provides a way to its interpretation.

4.2 Diffraction conditions

The purpose of this section is to describe the geometric conditions under which constructive interference of radiation scattered from a triply periodic arrangement of material units takes place. These conditions, known as diffraction conditions, are the basis of any experiment in which intensities of diffracted radiation are measured. These measurements have many purposes but two are outstandingly important: (i) to determine the periodicity, symmetry, and orientation of a crystal, and (ii) to obtain accurate estimates of the intensities of diffracted radiation, in order to elucidate from them the atomic arrangement within the asymmetric unit or, in other words, to determine its structure. Most usually, stage (ii) must be preceded by the completion of stage (i), but there are some important applications for which stage (i) is sufficient.

A more complete model of the structure of a material unit, and its effect on the diffraction pattern, will be considered in the next chapter. However, for the present purpose the simplest model, of classical electrons, each located at a lattice point and neutralized by a proton located nearby, will be considered. It will be seen in the next chapter how the mass of the proton makes its contribution negligible. This model is clearly a triply periodic arrangement of scatterers and suffices for the determination of the directions of the diffracted beams. No quantitative considerations of the intensities will be given.

4.2.1 The Laue and Bragg equations

Let us assume that the above “crystal” of point charges is irradiated with monochromatic X-radiation. Since X-rays are electromagnetic radiation, they can be described, at a large distance from the source, in terms of plane waves, with appropriate wavevectors. The electric field of the incident X-ray wave varies with time and therefore accelerates the point charges it encounters. Electromagnetic theory tells us that an accelerated charge emits energy in the form of electromagnetic radiation, with the same frequency as that of the incident wave. This may require some small correction for quantum effects, such as the Compton effect, but these will be neglected in the present treatment. We can therefore say that the incident X-rays are reemitted, with an unchanged wavelength, the efficiency of this reemission being determined by the scattering cross section of the electron for electromagnetic radiation. This topic will be dealt with in the next chapter.

We consider an X-ray wave, with wavevector \mathbf{s}_0 , falling on a crystal, and a reemitted (or scattered) X-ray wave with wavevector \mathbf{s} . In view of the assumption of unchanged wavelength, the magnitudes of the wavevectors \mathbf{s}_0 and \mathbf{s} will be identical, and we shall take them as

$$|\mathbf{s}| = |\mathbf{s}_0| = \frac{1}{\lambda}.$$

We assume further that the lattice of our crystal can be described in terms of the basis $(\mathbf{a} \ \mathbf{b} \ \mathbf{c})$. The question to be answered is: for what geometrical relationship

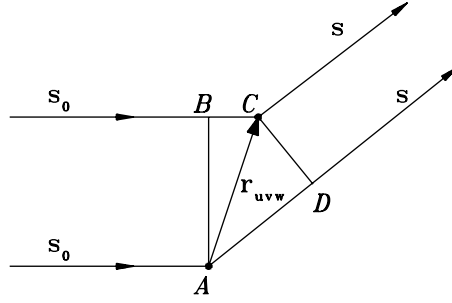


Fig. 4.1 Derivation of the Laue diffraction conditions.

between the wavevectors of the radiation and the basis vectors of the lattice will maximum constructive interference of the scattered X-ray waves occur? Because of the assumed strict periodicity of the arrangement, it is sufficient to consider two point charges related by translation through a lattice vector \mathbf{r}_{uvw} , as illustrated in Fig. 4.1.

The waves scattered from the charges at A and C will undergo maximum constructive interference if the difference between the optical paths passing through these charges is an integer multiple of the wavelength λ . It can be seen from Fig. 4.1 that the optical-paths difference is given by

$$\begin{aligned}\Delta &= AD - BC \\ &= \mathbf{r}_{uvw} \cdot \frac{\mathbf{s}}{|\mathbf{s}|} - \mathbf{r}_{uvw} \cdot \frac{\mathbf{s}_0}{|\mathbf{s}_0|} \\ &= \lambda \mathbf{r}_{uvw} \cdot (\mathbf{s} - \mathbf{s}_0).\end{aligned}$$

It follows that the required condition is

$$\mathbf{r}_{uvw} \cdot \mathbf{h} = \text{integer}, \quad (4.1)$$

where $\mathbf{h} = \mathbf{s} - \mathbf{s}_0$ is called the *diffraction vector*. This can also be rewritten as

$$(\mathbf{u}\mathbf{a} + \mathbf{v}\mathbf{b} + \mathbf{w}\mathbf{c}) \cdot \mathbf{h} = \text{integer}.$$

Since the coefficients u, v, w can be any integers, eqn (4.1) is equivalent to the three equations

$$\mathbf{a} \cdot \mathbf{h} = h \quad (4.2)$$

$$\mathbf{b} \cdot \mathbf{h} = k \quad (4.3)$$

$$\mathbf{c} \cdot \mathbf{h} = l, \quad (4.4)$$

which have to be simultaneously satisfied for maximum interference to occur; here h, k, l are any integers. Equations (4.2)–(4.4) are known as the Laue equations (Laue 1914).

In order to find a possible expression for the vector \mathbf{h} , let us divide both sides of each of the Laue equation by its right-hand side, and then subtract the second equation from the first, and the third from the second. We obtain

$$\left(\frac{\mathbf{a}}{h} - \frac{\mathbf{b}}{k}\right) \cdot \mathbf{h} = 0, \quad (4.5)$$

$$\left(\frac{\mathbf{b}}{k} - \frac{\mathbf{c}}{l}\right) \cdot \mathbf{h} = 0. \quad (4.6)$$

It can be seen that the vector \mathbf{h} is perpendicular to the vectors $\mathbf{a}/h - \mathbf{b}/k$ and $\mathbf{b}/k - \mathbf{c}/l$, and therefore also to the plane determined by these two vectors. It is also evident that the vector \mathbf{h} has the same direction as the vector product of these two vectors, that is, it is proportional to this product. We then have

$$\begin{aligned} \mathbf{h} &= K [(\mathbf{a}/h - \mathbf{b}/k) \times (\mathbf{b}/k - \mathbf{c}/l)] \\ &= K \left[\frac{\mathbf{b} \times \mathbf{c}}{kl} + \frac{\mathbf{c} \times \mathbf{a}}{lh} + \frac{\mathbf{a} \times \mathbf{b}}{hk} \right] \\ &\equiv p(\mathbf{b} \times \mathbf{c}) + q(\mathbf{c} \times \mathbf{a}) + r(\mathbf{a} \times \mathbf{b}). \end{aligned} \quad (4.7)$$

If we form the scalar products of both sides of eqn (4.7) with the vector \mathbf{a} , we obtain

$$\mathbf{a} \cdot \mathbf{h} = p\mathbf{a} \cdot (\mathbf{b} \times \mathbf{c}) = pV,$$

where V is the volume of the unit cell. If we use eqns (4.2)–(4.4), we obtain $p = h/V$ and, similarly, $q = k/V$ and $r = l/V$. It follows that

$$\mathbf{h} = h \frac{\mathbf{b} \times \mathbf{c}}{V} + k \frac{\mathbf{c} \times \mathbf{a}}{V} + l \frac{\mathbf{a} \times \mathbf{b}}{V},$$

that is, \mathbf{h} is a vector of the reciprocal lattice, as obtained from our discussion of lattice planes in Sections 1.2 and 1.3. This is a mathematical solution of the Laue equations.

Returning to the plane containing the vectors that appear in eqns (4.5) and (4.6), Fig. 4.2 shows that this is the plane whose intercepts on the coordinate axes are a/h , b/k , and c/l .

If we recall Section 1.2, we see that if h , k and l are relatively prime, this plane is just a lattice plane (hkl) , adjacent to the origin. If, however, h , k , and l have a common factor, say n , the plane is parallel to the $(h/n, k/n, l/n)$ family of lattice planes and belongs to a family of parallel and equidistant planes, in which only a plane the serial number of which is an integer multiple of n is a lattice plane. That is, if we write the indices of such a plane as $nh'nk'n'l'$, where $h'k'l'$ are relatively prime, we have for the interplanar distances

$$d_{nh'nk'n'l'} = \frac{1}{n} d_{h'k'l'}. \quad (4.8)$$

The interplanar distance (given by the distance of the plane in Fig. 4.2 from the origin) is, analogously to the calculation in Section 1.2,

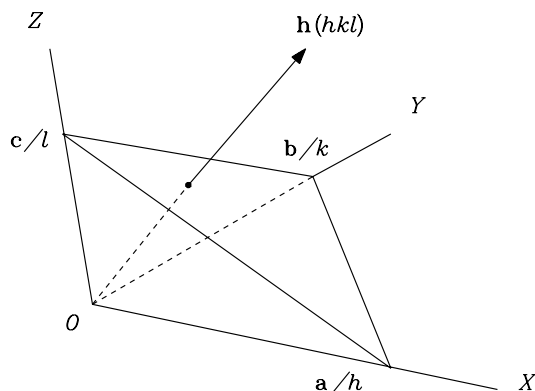


Fig. 4.2 Geometrical interpretation of Laue's equations

$$d_{hkl} = \frac{\mathbf{a} \cdot \mathbf{h}}{h} = \frac{1}{|\mathbf{h}|}, \quad (4.9)$$

since it follows from eqn (4.2) that $\mathbf{a} \cdot \mathbf{h}/h = 1$. If we now denote the angle between \mathbf{s} and \mathbf{s}_0 by 2θ , and construct the isosceles triangle obtained from $\mathbf{h} = \mathbf{s} - \mathbf{s}_0$, we have for $|\mathbf{h}|$

$$|\mathbf{h}| = |\mathbf{s}| \sin \theta + |\mathbf{s}_0| \sin \theta = \frac{2 \sin \theta}{\lambda}. \quad (4.10)$$

From eqns (4.9) and (4.10), we have

$$\lambda = 2d_{hkl} \sin \theta, \quad (4.11)$$

where h, k, l can be any integers. If h, k, l are of the form nh', nk', nl' , where h', k', l' are relatively prime and if we use eqn (4.8), we have

$$n\lambda = 2d_{h'k'l'} \sin \theta. \quad (4.12)$$

Equation (4.12) is the original version of the Bragg equation, and eqn (4.11) is the version most often encountered in practical applications. This is in fact a simpler interpretation of the Laue equations, in terms of a known wavelength, a single measurable scattering angle, and the interplanar spacing of the (hkl) family of planes. The interrelation of the geometry of lattice planes and the geometry of diffraction phenomena is quite remarkable.

Equations analogous to the Laue equations were already encountered in Exercise 3 in Chapter 1, in connection with the discussion of lattice planes and the reciprocal lattice. It is most significant that the diffraction vector \mathbf{h} satisfying the Laue's equations can be represented as a reciprocal-lattice vector. This result is widely employed in the theory and practice of diffraction from crystals.

4.2.2 Ewald's sphere of reflection

A highly suggestive geometrical description of the conditions for diffraction was put forward by Ewald (1913), and is employed very extensively in the crystallographic literature, albeit in several differing representations.

Let us first find the maximum value of $|\mathbf{h}|$. From eqn (4.11),

$$|\mathbf{h}| = \frac{1}{d_{hkl}} = \frac{2}{\lambda} \sin \theta$$

and since the maximum value of $\sin \theta$ is 1, we must have

$$|\mathbf{h}|_{\max} = \frac{2}{\lambda}.$$

Hence, all the reciprocal-lattice vectors potentially satisfying the Laue or Bragg equations, must be enclosed in a sphere of radius $2/\lambda$, with the origin of the reciprocal lattice chosen at the center of this sphere. This sphere is called the *limiting sphere* (see Fig. 4.3 and also the Exercises).

The Ewald sphere fits into the limiting sphere as indicated in Fig. 4.3. This is a sphere tangent to the limiting sphere at the point A and passing through the point O , the origin of the reciprocal lattice. Its radius is $1/\lambda$, and the incident beam, with wavevector \mathbf{s}_0 , is directed along the diameter AO . The wavevectors \mathbf{s} of the scattered radiation propagate from the point C , the center of the Ewald sphere, to the surface of that sphere.

It is convenient to imagine the crystal to be associated with the point C ; the fact that the spheres exist in reciprocal space and the crystal in the direct space should not give rise to difficulties, since all the reciprocal-lattice vectors involved have directions which are measurable in direct space, and magnitudes expressible in units of $(\text{length})^{-1}$ but calculable from direct-space quantities.

In a diffraction experiment carried out with monochromatic radiation, the Ewald sphere can either be fixed or be constrained to move within the limiting sphere while always passing through the point O and touching the limiting sphere from the inside. In either case, the triangle COP , built from the vectors \mathbf{s}_0 , \mathbf{s} and $\mathbf{s} - \mathbf{s}_0$ must be isosceles, but the vector $\mathbf{s} - \mathbf{s}_0$ is a diffraction vector *only* if it satisfies simultaneously the Laue equations or, equivalently, if the angle enclosed between \mathbf{s} , and \mathbf{s}_0 is twice the angle appearing in the Bragg equation. If this is the case, P is a point in the reciprocal lattice. Conversely, if a reciprocal lattice point comes into contact with the Ewald sphere, this point corresponds to a diffracted beam. This is the main idea of Ewald's most useful construction.

A diffracted beam is more often than not, called a reflection. The reason for this can be conveniently illustrated by the Ewald sphere. If the point P in Fig. 4.3 is a reciprocal-lattice point, the vector $\mathbf{h} = \mathbf{s} - \mathbf{s}_0$ is perpendicular to a family of lattice planes (hkl) in the crystal. The plane passing through the segment AP and perpendicular to the plane of the drawing is also parallel to the (hkl) family, since APO is of necessity a right angle (it is subtended by the diameter AO). If we shift this plane parallel to itself to the point C , it is seen that the angle

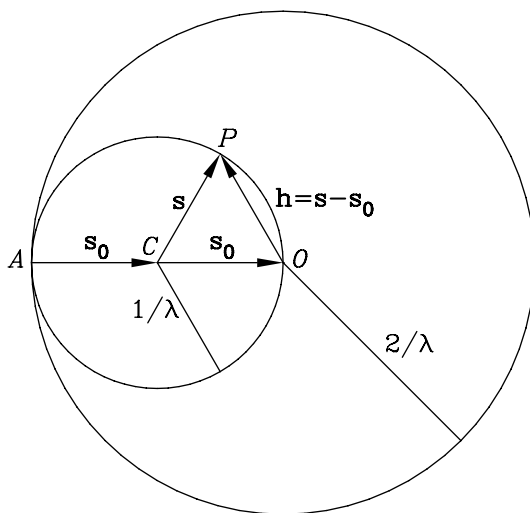


Fig. 4.3 The Ewald sphere.

formed by \mathbf{s}_0 and the plane is the same as the angle formed by the plane with \mathbf{s} and that each of these angles equals θ , the Bragg angle. A diffracted beam can therefore be represented pictorially as a reflection from a family of lattice planes and its orders (the integer n on the left-hand side of the Bragg equation, eqn (4.12), is called the order of the reflection). For the above reason, the Ewald sphere is widely known as the *sphere of reflection*. Obviously, the analogy with reflection of electromagnetic radiation from a mirror is only qualitative.

4.3 Production of X-rays

4.3.1 The X-ray tube

The traditional method of producing X-rays in a crystallographic laboratory is by means of an X-ray tube. This device, originally invented by Roentgen in 1895, and improved technically during the following century, is still being used and has an interesting physical background that marks major scientific developments. The principle of its operation is also very instructive.

An X-ray tube (see Fig. 4.4) consists of a tungsten filament, and a water-cooled metallic cup, both components being enclosed in an evacuated housing. The filament is connected to a source of alternating current (of the order of 10 A) and is, accordingly, heated. As a result of this, thermionic emission of electrons from the surface of the filament takes place—initially in all directions. When, however, a high voltage (of the order of 50 kV) is placed between the filament and the metallic cup, where the cup is grounded, the electrons emitted from the

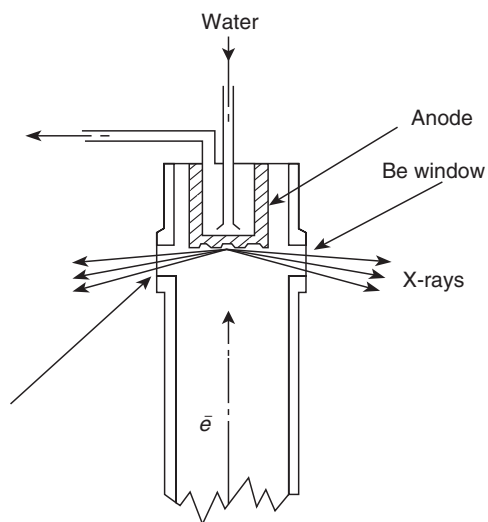


Fig. 4.4 Schematic drawing of an X-ray tube. Reproduced with copyright permission of the International Union of Crystallography (IUCr).

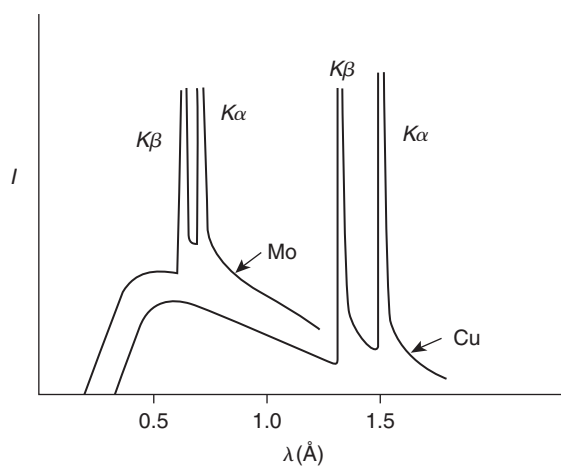


Fig. 4.5 Parts of the X-ray spectra from copper and molybdenum anodes. Reproduced with copyright permission of the International Union of Crystallography (IUCr).

filament are sharply focused in the direction of the cup. When these electrons collide with the cup (the anode), most of their kinetic energy is converted into heat—and hence the necessity for cooling the cup. The remaining part is converted into radiative energy, which was called *X-rays* by Roentgen, the “X” standing for something not understood. This radiation leaves the X-ray tube through thin

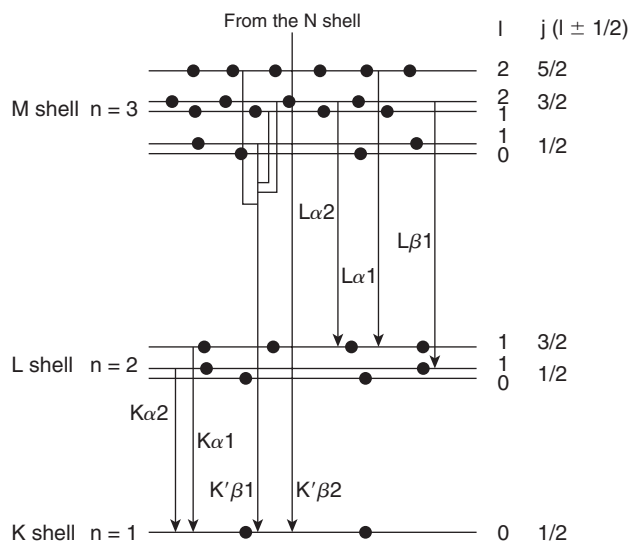


Fig. 4.6 *Electronic transitions and characteristic radiation.* Reproduced from the web site: <http://ie.lbl.gov/xray/>.

windows, usually made from beryllium.

Parts of the spectra of X-radiation obtained from collisions of electron beams with copper and molybdenum cups are illustrated in Fig. 4.5. In both cases we see a continuous broad “hill” and two sharp peaks superimposed on it, the second sharp peak appearing at wavelength of about 0.7 and 1.5 Å for molybdenum and copper, respectively. More sophisticated arrangements may show additional sharp peaks, which, however, are of little relevance for our purposes.

There obviously exists some shortest wavelength at which radiation is obtained. When an electron of charge e under a potential difference of V volts is brought to a halt at the surface of the anode, it is suddenly decelerated (negatively accelerated), and its energy eV is transformed into the energy of an X-ray photon $h\nu$, where h is Planck’s constant and ν is the photon’s frequency. For the highest frequency of the photon, or its lowest wavelength, we have

$$eV = h\nu_{\max} = \frac{hc}{\lambda_{\min}} \quad \text{and} \quad \lambda_{\min} = \frac{hc}{eV} \approx \frac{12\,400}{V}.$$

For example, for $V = 50\,000$ volts we shall have $\lambda_{\min} \approx 0.25$ Å. An explanation of the intensity distribution within the broad hill will not be given here but it is clear that it depends on the accelerating voltage in the tube. This broad hill of radiation intensity, called *white radiation*, was thought for many years to be of little use but, as we shall see later, it is most useful with the Laue method.

Table 4.1 Some frequently applied wavelengths (in Ångstrom units).

Copper:	wavelength (Å)
$\lambda(K\beta)$	1.3922
$\lambda(K\alpha_1)$	1.5406
$\lambda(K\alpha_1)$	1.5444
$\lambda(K\alpha_{av})$	1.5418
Molybdenum:	wavelength (Å)
$\lambda(K\beta)$	0.6323
$\lambda(K\alpha_1)$	0.7093
$\lambda(K\alpha_1)$	0.7136
$\lambda(K\alpha_{av})$	0.7107

The sharp peaks are known as the *characteristic radiation* and the wavelengths at which they appear depend on the element from which the anode is constructed. They are, in fact, related to the energetic structure of the atoms of that element, as will be explained below. When an electron retains just enough energy to be able to ionize the lowest-lying shell in an atom of the anode, an electron with principal quantum number $n = 1$ is raised to the continuum and gives rise to transitions of electrons from higher energy levels to the lowest level. Upon such a transition, a photon is emitted with an energy related almost exactly to the levels involved. X-ray spectroscopy associates the quantum numbers $n = 1, 2, 3, 4$ etc. with the letters K, L, M, N etc, as seen in Fig. 4.6. Thus, the origin of the sharp peak labeled $K\beta$ in Figure 4.5 is several transitions from the M shell and also some from the N shell. They appear as one sharp peak in all but very high-resolution measurements. The peak labeled $K\alpha$ appears as a single peak at low or moderate scattering angles and as a doublet at high scattering angles: $K\alpha_1$ associated with a transition from the L shell, with $l = 1$ and spin $+1/2$, to the K shell, and $K\alpha_2$ associated with a transition from the L shell, with $l = 1$ and spin $-1/2$, to the K shell. This doublet is employed in crystallographic experiments aimed at very accurate determination of unit cell constants, but the most frequently employed wavelength is that corresponding to a weighted average of $\lambda(K\alpha_1)$ and $\lambda(K\alpha_2)$. Table 4.1 lists the wavelengths of special interest in routine crystallographic studies; these concern anodes made from copper and molybdenum. A comprehensive list of interesting wavelengths as well as detailed information on the properties of X-rays, is given in Chapter 4.2 of Volume C of the *International Tables for Crystallography* (Wilson and Prince 1999). The other transitions indicated in Fig. 4.6 give rise to radiation with longer wavelengths, lower intensity and which is much more readily absorbable.

More or less approximate monochromatization

Apart from the Laue method, to be discussed later, all diffraction techniques are based on the assumption that the radiation used is approximately monochro-

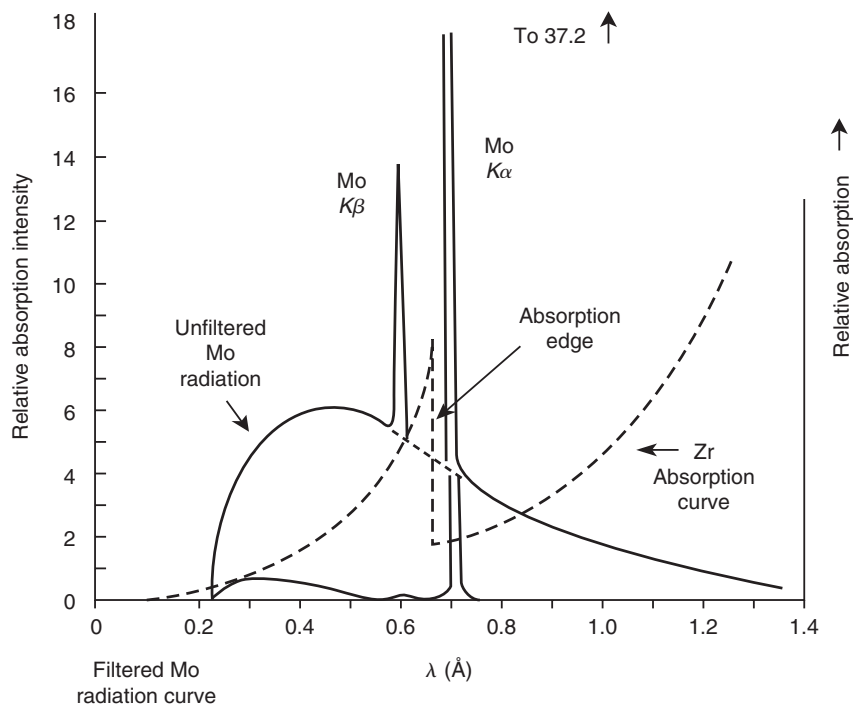


Fig. 4.7 Molybdenum radiation approximately monochromatized with a zirconium filter. Reproduced with copyright permission of the International Union of Crystallography (IUCr).

matic. The most intense characteristic radiation is $K\alpha_1$, or $K\alpha_{av}$ if a limited angular range of the scattering is available. Therefore, one seeks to suppress the radiation at all wavelengths except in a narrow range around the required wavelength. This can be quite usefully, if not completely, done by using a thin foil of a material which has an absorption edge (see below) at a wavelength somewhat shorter than $\lambda(K\alpha)$. If the atomic number of the metal from which the anode is made is Z , that of the filter material should be $Z - 1$ or $Z - 2$. Thus, nickel foil is used as a filter for copper radiation and zirconium for molybdenum radiation. Figure 4.7 shows the effect of a zirconium filter on the X-rays emitted from a molybdenum anode. Note the location of the absorption edge in the absorption spectrum of zirconium.

The above filtering method will now be briefly explained. X-rays are absorbed in matter according to Beer's law,

$$I = I_0 \exp(-\mu t),$$

where I_0 is the incident intensity of the X-ray beam, μ is the linear absorption

coefficient, t is the thickness of the irradiated specimen, and I is the intensity of the X-ray beam after it has passed through the specimen. This law is applicable to electromagnetic radiation in general. The absorption coefficient depends on the wavelength of the incident radiation, and in the case of X-rays, for a single atomic species (for example nickel atoms) it depends on the atomic number and on the third power of λ . Hence the absorption increases with increasing λ . However, when an energy is reached which corresponds exactly to the ionization energy of an atom in the absorber, the absorption falls abruptly and then continues to increase again as λ increases. The X-ray absorption spectrum of an atom has a sawtooth shape, each peak corresponding to the ionization of an electron from one of the atomic energy levels. The abrupt decrease of the absorption is called an absorption edge. For example, in the case of nickel the wavelength of the K absorption edge (corresponding to the ionization of the K shell) is $\lambda = 1.4882 \text{ \AA}$. Such a filter obviously decreases the $\text{Cu}(K\alpha_{\text{av}})$ emission line but suppresses the $\text{Cu}(K\beta)$ and the white radiation to a much greater extent. Optimization of the filter thickness is of crucial importance here.

The above approximate monochromatization method is cheap, elegant, but rather imperfect and is only very infrequently used nowadays. A much more accurate method, is the use of a crystal monochromator. The principle is simple. A crystal is mounted in the incident X-ray beam so that its strongest reflection for a chosen wavelength, is active. The X-ray beam diffracted from the crystal is then used as the incident beam that falls on the sample to be examined. The wavelength of that radiation is just the above chosen wavelength. This is good but not entirely exact because of the width of the reflection profile from the monochromating crystal. There is another problem, that of harmonics: as we know, the Bragg equation is

$$n\lambda = 2d_{hkl} \sin \theta,$$

where $n = 1, 2, 3, \dots$ is the order of the reflection from the lattice plane (hkl). Hence, together with radiation of wavelength λ , reflections corresponding to $\lambda/2$, $\lambda/3$, etc. may also be obtained. However, this can usually be taken care of either by an appropriate choice of the monochromator crystal or during the processing of the data.

4.3.2 Synchrotron radiation

All the diffraction techniques to be outlined below are of widespread availability; they can be found in crystallographic laboratories, and serve as the basic tools for the collection of diffracted-intensity data. A popular instrument is the four-circle diffractometer, because of its accuracy and sophisticated automation. Its main limitations, when a sealed X-ray tube is used, are the relatively low intensity of incident radiation that can be obtained and the necessity for collecting the diffracted intensities from one reflection at a time. The first of these results in time-consuming experiments, and the second adds the danger of crystal deterioration due to radiation damage. Ideally, therefore, one would like to be able to

collect a large number of diffracted intensities in a short time. The best answer to the latter requirement is offered by synchrotron radiation which is produced in special installations. The simultaneous collection of several items of intensity data is made possible by area detectors (see below).

The physical principle of synchrotron radiation goes back to classical electrodynamics: an accelerated moving charge emits a spectrum of electromagnetic energy, and if the magnitude of the velocity of its motion is comparable to the speed of light, very significant effects are predicted and, in fact, observed. The theory of synchrotron radiation and its application to crystallography have been discussed rather extensively in the literature (for example Koch 1983; Coppens 1992), and only a brief outline will be given in this chapter. If a charge e moves with a velocity \mathbf{u} , and has an acceleration vector $\dot{\mathbf{u}}$, then the power radiated by the charge is given by

$$P = \frac{e^2}{6\pi\epsilon_0 c^3} \frac{\dot{u}^2 - (\mathbf{u} \times \dot{\mathbf{u}})^2/c^2}{(1 - u^2/c^2)^3}, \quad (4.13)$$

(Schwinger 1949; Panofsky and Phillips 1956), where c is the speed of light in vacuo and ϵ_0 is the permittivity of free space. This general expression readily admits the basic ideal features of the synchrotron as a special case: a charge rotates in a circular orbit of radius R with speed u , caused by a strong magnetic field perpendicular to the plane of the orbit, and orbits with a constant circular frequency ω . At any instant the velocity vector is tangential to the orbit, and the acceleration vector is perpendicular to it. Hence the magnitude of the vector product $(\mathbf{u} \times \dot{\mathbf{u}})$ reduces to $u\dot{u}$ and eqn (4.13) can be rewritten as

$$P = \frac{e^2 \dot{u}^2}{6\pi\epsilon_0 c^3} \frac{1}{(1 - u^2/c^2)^2}. \quad (4.14)$$

It is readily seen that for speeds much lower than c , eqn (4.14) reduces to

$$P = \frac{e^2 \dot{u}^2}{6\pi\epsilon_0 c^3} \quad (4.15)$$

which is the total instantaneous power radiated by a nonrelativistic accelerated charge. Equation (4.15) is of importance in the description of the scattering of X-rays by electrons in a crystal, since relatively small speeds are involved. This will be discussed in some detail in the next chapter.

Returning to eqn (4.14) and the acceleration of a charge in circular motion, the magnitude of the acceleration is $R\omega^2$, and if we introduce the definitions $\beta' = u/c$ and $\gamma' = (1 - \beta'^2)^{-1/2}$, eqn (4.14) becomes

$$P = \frac{e^2 R^2 \omega^4 \gamma'^4}{6\pi\epsilon_0 c^3}. \quad (4.16)$$

Since, further, $\omega = u/R = c\beta'/R$, we can write

$$P = \frac{e^2 c}{6\pi\epsilon_0} \frac{\beta'^4 \gamma'^4}{R^2}. \quad (4.17)$$

The total instantaneous power radiated by an electron accelerated in this way is therefore approximately proportional to the fourth power of the energy of the relativistic electron. In fact, the parameter γ' can be written as the ratio of the energy of the moving electron to its rest energy, and the speed-dependent term β'^4 tends to unity as u tends to c . Very high speeds permit large values of the radius and hence an ample circumference of the orbit, which allows a large number of users to benefit from this radiating accelerator. As will be seen later, the radiated power is very much higher than that obtainable from conventional sources, such as X-ray tubes with stationary or even rotating anodes.

The above description forms the theoretical basis of real synchrotron installations, which have led to major breakthroughs in structural studies. Detailed descriptions of the principles of operation of real synchrotrons and their application to crystallographic research are given in Coppens' (1992) and many other sources in the literature. We shall outline these principles briefly in what follows. We show in Fig. 4.8 a schematic view of an actual synchrotron installation.

- Electrons are injected by an electron gun into a linear accelerator (LINAC) in which they reach an energy of several hundred million electron volts (MeV).
- These energetic electrons are then injected into a synchrotron (BOOSTER), in which they circulate rapidly, while gaining an amount of energy in each revolution. This continues until the electrons reach an energy of several billion electron volts (GeV). At this point the speed of the electrons is very close to the speed of light c , and the parameter γ defined above becomes enormously large.
- These highly energetic electrons are then extracted from the synchrotron into the storage ring, where their motion is maintained, and they are therefore continuously accelerated and emit, tangentially to the ring, a spectrum of intense electromagnetic radiation.

A detailed description of the various experimental installations shown in Fig. 4.8 is outside the scope of this chapter. We shall just point out that many of them deal with extensive crystallographic research and they are well described on the web site http://www.aps.anl.gov/About/Research_Teams. It is also in order to point out that while APS is a major synchrotron installation, an increasing number of such installations can now be found in many countries.

A most important consideration is the spectral distribution of the synchrotron radiation, and specifically the achievement of high intensities of radiation in the interesting range of wavelengths—particularly those corresponding to X-rays. In practical installations, this is taken care of by suitable modifications of the path of the electron beam, and hence enhanced acceleration, with the aid of the insertion devices (see, for example, Coppens, 1992).

THE ADVANCED PHOTON SOURCE

Sector Allocations & Disciplines Source Configuration

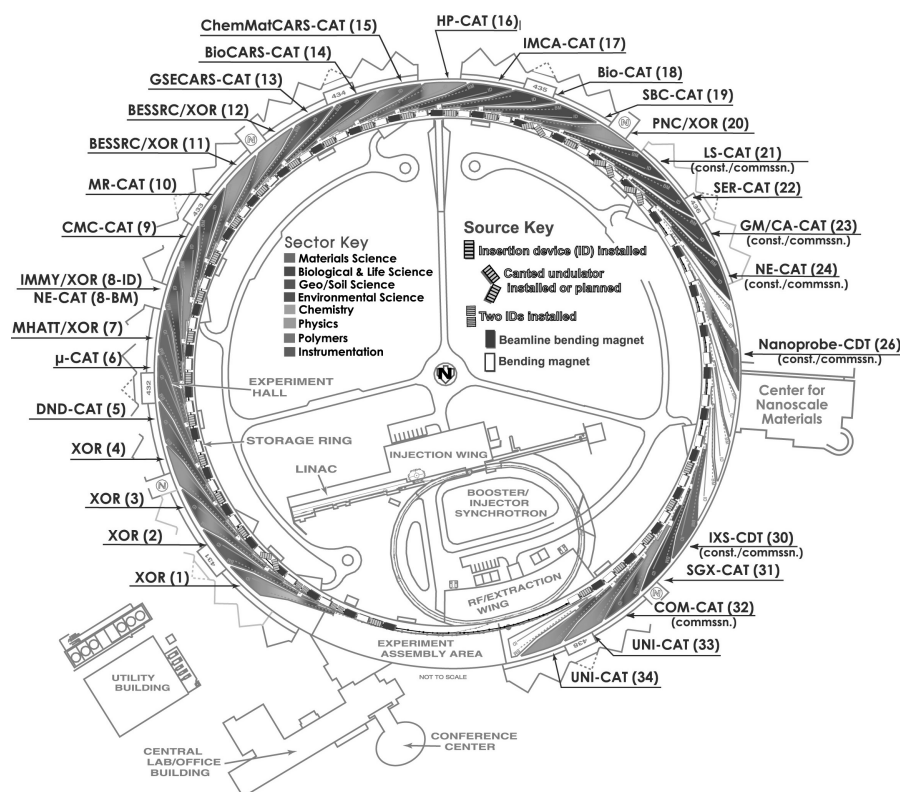


Fig. 4.8 A general view of the APS synchrotron. The symbols around the storage ring refer to different experimental installations which make use of the synchrotron radiation (see text). Reproduced by courtesy of the Argonne National Laboratory.

Last but not least, a comparison of brilliance between conventional X-ray tubes and synchrotrons, as given in Fig. 4.9, brings out the main reason for the usefulness of this electron accelerator. (Brilliance is a quantity related to intensity (the average energy per unit time, per unit area) but also depends on the degree of spectral purity of the radiation, and has served until recently as a unit of comparison between various radiations.) It can be seen from Fig. 4.9 that no significant progress was made in the enhancement of the brilliance of X-ray sources from the invention of the X-ray tube by Roentgen in 1895 until about 1960. In the early 1960s, an X-ray tube with a rotating anode was introduced, which gave rise to an increase in the brilliance by an order of magnitude. This was

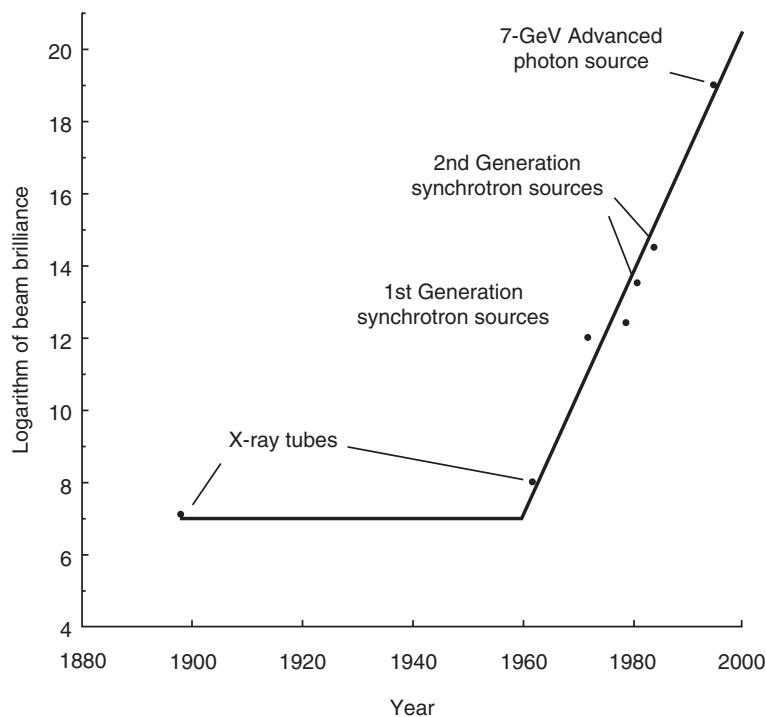


Fig. 4.9 *History of X-rays.* Reproduced by courtesy of Dr. R. Garrett from the web site: <http://www.ansto.gov.au/natfac/asrp4.html>.

regarded as a major development, but not for very long. The real breakthrough was afforded by particle accelerators in which *unwanted* synchrotron radiation from the electrons present was detected. This was accompanied by an increase in the brilliance by several orders of magnitude and marked the beginning of the so-called first-generation synchrotrons. It was soon realized that a program of construction of electron accelerators dedicated to the production of synchrotron radiation was indicated, and a second generation of synchrotrons appeared, with a marked increase in brilliance. Further attempts were made at enhancing the brilliance by introducing various insertion devices, which contribute to increased acceleration of the electrons in the storage ring, and by improving the maintenance of their energy—this led to the third-generation synchrotrons. Further research is in progress but even that accomplished some years ago has led to an increase in the brilliance by a factor of about 10^{12} as compared with a sealed X-ray tube with a rotating anode. This development is responsible for major advances in the structure determination of protein crystals and for the introduction of a variety of techniques which became feasible given the high brilliance of the radiation.

It should be pointed out that synchrotron radiation ranges throughout most of the useful spectrum of electromagnetic radiation, and thus constitutes a major stimulus to experimental science.

4.4 Detectors of X-rays

This section describes briefly the principles of operation of some detectors of X-rays that used to be or still are very popular. More detailed descriptions of these and other detectors, accompanied by graphical presentations and many references to relevant literature, are given in Volume C of the *International Tables for Crystallography* (Amemiya et al., 1999).

4.4.1 X-ray film

The oldest detector of X-rays, and one which is being used in many laboratories to this very day, is photographic film. Its principle of operation and processing are well known, but we shall recall them for the sake of completeness. X-ray film, unlike conventional photographic film, is coated on *both* sides with an emulsion, in which predominantly ionic silver halide crystals (usually AgBr) are dispersed.

- When an X-ray photon strikes the film, a small number of silver ions in an excited crystallite are converted to black metallic silver. So, upon completion of the experiment, a latent image of the diffraction pattern is stored in the film.
- The conversion process to metallic silver (only in the silver halide crystals exposed to X-rays) is completed by the developer solution, and the pattern of scattered X-rays which reached the film appears as appropriate blackenings on the emulsion. All this process is of course performed in a darkroom, to prevent exposure of the film to visible light.
- After the film has been washed in order to remove unwanted reaction products and traces of the developer solution, it is immersed in a fixer bath. The purpose of fixing is to remove the emulsion and all the silver halide crystals that were not exposed to X-rays. One now has (after washing and drying) a transparent film showing diffraction spots, the positions and relative intensities of which can be measured for the purpose of structure determination.

The positions of the spots are fairly accurate and can be used for a good determination of the unit cell parameters. However, the blackening of the film is proportional to the intensity of X-rays that caused it only in a relatively small range, called the linear range of optical density. If the whole range of optical densities was to be measured, it was customary to work with packs of several films: the weak reflections were measured on the film facing the incoming scattered radiation, and the intensity of the strongest reflections was reduced to the linear range in the last film of the pack. Although this procedure is rather tedious, this disadvantage is mainly technical. A more serious shortcoming is the very low quantum efficiency of X-ray film, which results in the need for very long exposures. The quantum efficiency of a detector is defined as the ratio of

the number of detections to the number of incident photons. In the case of X-ray film, a detection can be taken as the excitation of a silver halide crystal, and the quantum efficiency amounts here to a few percent.

4.4.2 Imaging plate

The imaging plate is an area detector, qualitatively similar to the photographic film but operating on entirely different principles. It also consists of a support coated with an emulsion, which, however, contains crystallites of barium fluoride bromide or barium fluoride iodide with artificially introduced impurities of Eu^{2+} (doubly ionized europium). During the preparation of these crystals a large number of vacancies is created at the sites of fluoride and bromide (or iodide) negative ions, and these vacancies are essential to the process (see below).

- When a photon strikes the imaging plate, Eu^{2+} ions are ionized further to Eu^{3+} and the “detached” electrons are raised to the conduction band. When so excited, the electrons are trapped at the vacancies and thereby produce temporary color centers. Hence, the imaging plate changes color at the sites on which incident scattered radiation is falling.
- When the exposure has been completed, the diffraction pattern has been temporarily recorded on the imaging plate. The plate is then scanned by a He–Ne laser, and the trapped electrons are released, fall down to the valence band, and recombine with Eu^{3+} to Eu^{2+} . This transition is accompanied by a release of energy, which corresponds to the emission of blue light. The intensity of this luminescence, measured with a photomultiplier, is proportional to the intensity of the X-rays which gave rise to the color centers.
- The coordinates of the diffraction spots and the intensity of the luminescence are recorded online in a computer and constitute the required set of data. When the scanning process has been completed, the imaging plate is exposed to visible light, which erases all the remaining traces of color centers and the plate is suitable for further use.

Unlike the X-ray film discussed above, the imaging plate has a very large linearity range, and an excellent quantum efficiency, and is therefore a convenient and very fast detector of X-ray diffraction patterns. It is nowadays frequently used in the collection of intensity data from protein crystals and is quite popular in other applications.

4.4.3 Charge-coupled device (CCD) detector

Another powerful area detector is based on a popular method of electronic imaging, which employs a two-dimensional array of small light-sensitive elements, known as a charge-coupled device; the elements are referred to as pixels. The CCD has a variety of applications, and their implementation in an X-ray detector is discussed by Amemiya et al. (1999) and in the literature referred to there. Let us see, in broad outline, how X-rays scattered from a crystal are converted into an image of a diffraction pattern.

- The detector itself has the shape of a truncated cone, at the large base of which is a phosphor screen, the purpose of which is to convert incident X-ray photons into visible light. The light emitted by the screen is conducted by a tapered bundle of optical fibers and strikes the array of pixels, each of which is a metal–oxide–semiconductor (MOS) capacitor.
- When a light photon strikes an MOS pixel, an electron is emitted owing to the photoelectric effect and stored in the capacitor (an electron–hole pair is produced). Therefore, the charge distribution throughout the whole CCD follows the distribution of radiation scattered from the crystal. The charge is subsequently transferred to an electronic circuit, and converted into an array of pulses the height of which is proportional to the intensity of X-rays that fell on the phosphor screen. This digital information is transferred to a computer, which records the pattern of diffracted intensity on a relative scale.
- The crystal is then rotated, new reciprocal-lattice vectors come into contact with the Ewald sphere, and a new charge frame is produced in the CCD. All this is repeated until the desired portion of the diffraction space has been covered by the motions imparted to the crystal. The required information on the distribution of diffracted intensity is now stored in the computer and available for further processing.

The CCD detector has a very large linearity range; it has a high quantum efficiency and a large dynamic range (the ratio between the maximum and minimum reliably measured intensities). It is not clear whether the imaging plate or the CCD detector is preferable, but both are certainly in the forefront of intensity data collection. The performance of the CCD detector also depends on the size of the pixel array. Typical values are 1.5 to about 4 million pixels. Interestingly, values of the same order are encountered in digital cameras, in which CCD arrays have replaced photographic film.

4.5 The rotating-crystal method

This is the oldest moving-crystal method. It was for many decades associated with photographic film and conventional X-ray tubes, but in modern research the X-ray film is being replaced by imaging plates and—where feasible—the X-ray tube by synchrotron radiation. However, this has nothing to do with the geometrical considerations of this method, and an important variant of it, the oscillation method.

The diffraction condition is fulfilled when a point of the reciprocal lattice comes into contact with the sphere of reflection. If the radiation is monochromatic and the crystal is stationary, any occurrence of reflections is accidental and there may be none at all. Since the direct lattice can be represented in terms of families of parallel, equidistant lattice planes, and to each of these families there correspond collinear vectors in the reciprocal lattice, then if the crystal is rotated about some direction, a large number of reciprocal-lattice vectors will

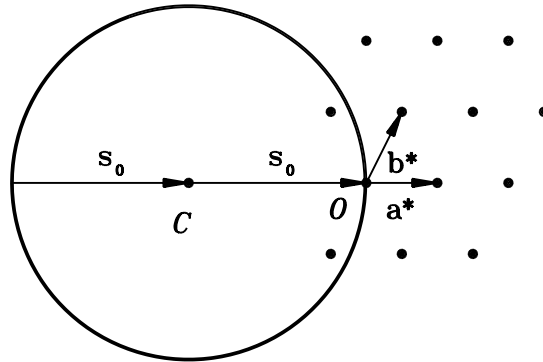


Fig. 4.10 Rotating crystal method. Schematic drawing.

sweep through Ewald's sphere and give rise to reflections. This is the principle of the rotating crystal method, and is related to other methods in which the crystal is moved in order to bring reciprocal-lattice points into contact with the sphere of reflection. Let us consider Figure 4.10. The plane of the drawing contains the basis vectors \mathbf{a}^* and \mathbf{b}^* of the reciprocal lattice and linear combinations of them with integer coefficients, and the direct basis vector perpendicular to this lattice plane in the reciprocal lattice must be the vector \mathbf{c} (see Section 1.3).

Consider the Laue equation $\mathbf{c} \cdot \mathbf{h} = l$, with $l = 0$. The locus of the vectors \mathbf{h} (not only that of their endpoints) is a reciprocal-lattice plane perpendicular to \mathbf{c} , that is, a typical diffraction vector has the form $\mathbf{h} = h\mathbf{a}^* + k\mathbf{b}^* + 0\mathbf{c}^*$, and each of the reciprocal-lattice points in this plane has indices $hk0$. When the crystal is rotated about \mathbf{c} , each of the points with indices $hk0$ becomes a *reflection* $hk0$ as soon as the endpoint of the reciprocal-lattice vector $h\mathbf{a}^* + k\mathbf{b}^* + 0\mathbf{c}^*$ comes into contact with the surface of the sphere of reflection. The diffracted beams radiate from the point C and lie in the $(\mathbf{a}^*, \mathbf{b}^*)$ plane. They can also be regarded as lying on the surface of a flat cone, with the apex at the point C .

We now proceed to the Laue equations $\mathbf{c} \cdot \mathbf{h} = l$ with $l \neq 0$. If we divide both sides of this equation by $c = |\mathbf{c}|$, we obtain

$$\frac{\mathbf{c}}{c} \cdot \mathbf{h} = \frac{l}{c}, \quad (4.18)$$

that is, the projection of \mathbf{h} on the direction of \mathbf{c} is constant and equals l/c . The locus of the endpoints of \mathbf{h} , satisfying eqn (4.18), is a plane in the reciprocal lattice in which each point has indices hkl . As the crystal rotates about \mathbf{c} , the vectors \mathbf{h}_{hkl} , for l not exceeding a certain maximum value, cross the sphere of reflection and give rise to corresponding diffracted beams. These beams, or

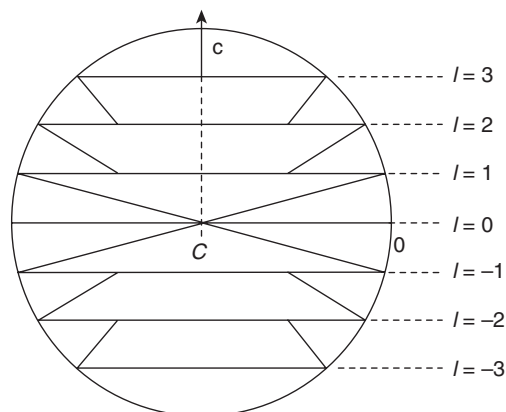


Fig. 4.11 Projected Laue cones limited by the Ewald sphere.

reflections, are located on the envelope of a cone with its apex at the point C , its axis parallel to the axis of rotation, and its half-opening angle given by

$$\alpha_l = \cos^{-1} \frac{l\lambda}{c}.$$

Clearly, the maximum value of l is c/λ , truncated to the nearest integer.

Each Laue equation therefore corresponds to a family of planes in the reciprocal lattice which, upon rotation of the crystal, intersect the sphere of reflection and form a series of reflection cones, known as *Laue cones*. Figure 4.11 illustrates this statement.

The rotating crystal method, the oldest technique employing monochromatic radiation, is related in a simple manner to the above description. Suppose that a single crystal is irradiated, with \mathbf{s}_0 perpendicular to \mathbf{c} , while it is rotating about the direction of \mathbf{c} at a uniform angular speed. Let us now surround the crystal with a cylindrical photographic film, suitably protected from exposure to light, so that the axis of rotation coincides with the axis of the cylinder. The Laue cones, or the loci of the reflections, will intersect the cylinder in circles on the circumference of which the X-ray reflections (assumed to penetrate the protecting medium) will give rise to latent sharp spots. After the experiment has been performed and the cylindrical film or other imaging medium has been flattened out, we obtain a series of straight rows of sharp spots, of varying degree of blackening.

The spots in the central row correspond to the Laue equation $\mathbf{c} \cdot \mathbf{h} = 0$ and therefore to indices $hk0$. The first row above the center has indices $hk1$, the first below the center has indices $hk\bar{1}$, and so on. A complete interpretation of the photograph would involve the assignment of indices h and k to each spot in the row of $hk0$ reflections (this turns out to be sufficient) and a quantitative estimation of the intensity of the spots in the photograph. Such an assignment

of indices, or *indexing*, requires a knowledge of unit cell parameters of the direct or reciprocal cell, and a single rotation photograph furnishes only one such parameter, as will be seen below. Let d be the distance of the l th circle on the film from the central row, and let R be the distance of the film from the crystal. Therefore,

$$2\theta = \tan^{-1} \left(\frac{d}{R} \right).$$

The distance from the base of the l th Laue cone from the flat cone, in the sphere of reflection, is l/c . We thus have

$$\frac{l/c}{1/\lambda} = \frac{l\lambda}{c} = \sin(2\theta)$$

and hence

$$c = \frac{l\lambda}{\sin[\tan^{-1}(d/R)]}$$

and only the length of the vector \mathbf{c} can be determined.

It should be pointed out that a rotation photograph of a cubic crystal can be readily indexed, since only one parameter is needed. However, for lower symmetries other types of information are usually required. The rotating-crystal method has been described here mainly in order to introduce the reader to the basics of the formation of a diffraction pattern. The actual experimental technique involved and further details of the interpretation are very clearly described for example, by Buerger (1941) and by Stout and Jensen (1968), and the interested reader is referred to these works.

4.6 Moving-crystal–moving-film methods

We shall now mention briefly some photographic methods that served as the crystallographer's tool for several decades, and some of which are still used, albeit not frequently. However, their revival is possible in view of the development of new, highly efficient, detectors which can replace the classical photographic film, as well as in view of the possibility of computerized indexing.

4.6.1 The Weissenberg method

Consider the arrangement described in the previous section, with two modifications: (i) only one Laue cone is allowed to reach the film, for example by the use of a sliding cylindrical metallic absorber with a circular slit that can be positioned so that only a desired cone is transmitted, and (ii) the cylindrical film is allowed to move back and forth, while remaining coaxial with the axis of rotation of the crystal; the movement of the film and the rotation of the crystal are synchronous (for example, Buerger, 1941). If, for example, only the $hk0$ Laue cone is allowed to pass, the $hk0$ reflections will be spread throughout the film in a regular manner and this turns out to permit the determination of the parameters a^* , b^* and the angle γ^* . So, from a single setting of the crystal, four out of the six possible

parameters can be determined. Further experimental details are provided in the references quoted.

4.6.2 The de Jong–Bouman method

In this method, very elegantly illustrated by Woolfson (1997), also only one Laue cone is allowed to pass. This is done by placing a flat metallic absorber with a circular ring aperture in a plane perpendicular to the axis of rotation of the crystal, say the \mathbf{c} axis, so that the axis is directed towards the center of the circular absorber. The Laue cone is selected by setting the inclination of \mathbf{s}_0 with respect to the \mathbf{c} axis, and the distance of the absorber from the crystal. A flat film is rotated about an axis parallel to the axis of rotation of the crystal at the same angular speed as the crystal, the plane of the film being perpendicular to the axis of rotation. In our example, the reflections $hk0$ are spread all over the film. However, if a crystal is rotated about an axis at a certain angular speed, the reciprocal lattice is rotated about a parallel axis with the same speed. Hence, the distribution of the spots on the de Jong–Bouman photograph will follow the geometry of the reciprocal-lattice plane based on \mathbf{a}^* and \mathbf{b}^* . This is the first example of the so-called “undistorted reciprocal-lattice photography”. In fact, the Weissenberg method also produces “photographs of the reciprocal lattice”, but seriously distorted ones owing to the cylindrical geometry.

4.6.3 The Buerger precession method

This method is described in great detail by Buerger (1964) and is dealt with more briefly in most crystallographic texts. In this method, again only one Laue cone is allowed to pass in a given experiment, and its result is an undistorted image of a reciprocal-lattice plane. However, the mechanical design is based on a precession—rather than rotation—of a direct lattice vector, a corresponding precession of the transmitted Laue cone and the absorber involved, and a rather complicated motion of the film involving a combination of precession and translation of the film parallel to itself. While the de Jong–Bouman principle illustrates reciprocal-lattice photography neatly, Buerger’s precession camera—although complicated—is versatile and much more frequently used. This is especially true for preliminary examinations of protein crystals.

4.7 The four-circle diffractometer

4.7.1 Geometrical considerations

An outstandingly important instrument, allowing one to determine the full set of unit-cell parameters as well as to measure accurately the intensities of all the accessible reflections—all with a single setting of the crystal—is the four-circle diffractometer. This instrument is equipped with a photon-counting device and a mechanical system which can be programmed (i) to bring the crystal into an orientation in which the wavevector of the incident radiation forms the Bragg angle θ with the desired plane hkl , and (ii) to bring the slit of the detector to a position in which it can receive the scattered radiation, with a wavevector *also* forming the Bragg angle θ with the plane hkl . This very general description

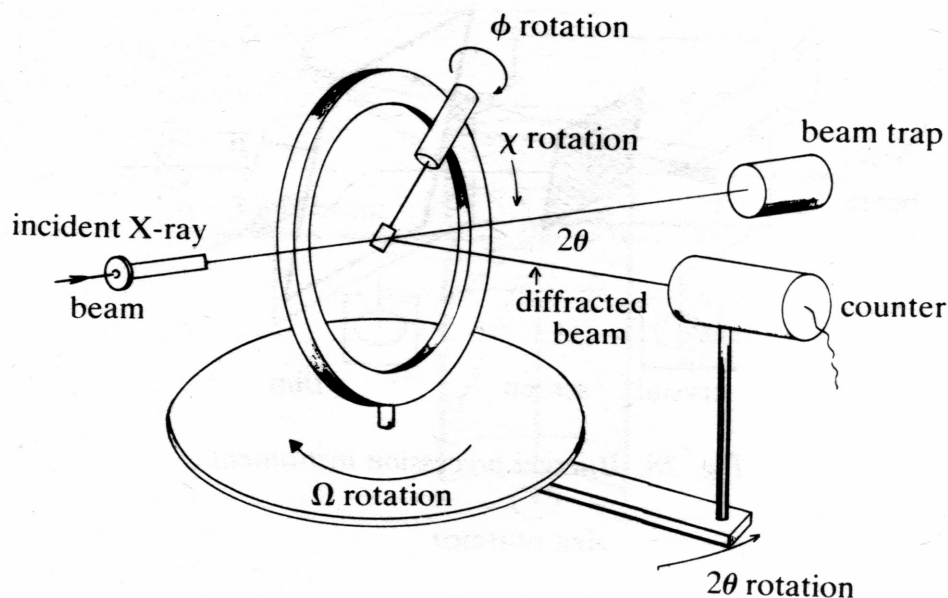


Fig. 4.12 A schematic drawing of a four-circle diffractometer. Reproduced with copyright permission of the International Union of Crystallography (IUCr).

indicates that the diffractometer can be programmed to measure automatically the intensities of a large range of reflections, which is an obvious asset. However, it also indicates that the reflections are measured one at a time, which is a disadvantage if the number of reflections is very large and the intensity of the scattered radiation deteriorates upon prolonged exposure of the crystal to X-rays. For this reason, and in order to perform the data collection more expediently, the slit that accepts one reflection at a time is being gradually replaced with an area detector such as, for example, the CCD device discussed above. The problem of crystal deterioration is encountered most often in studies of protein crystals, and is less acute in crystals of small and medium-sized molecules. Of course, the replacement of the slit with an area detector radically changes the computational aspects of the data collection, a detailed treatment of which is outside the scope of this book. We shall, by way of an introduction, analyze the classical four-circle diffractometer which measures one reflection at a time. The present analysis is based on the article by Hamilton (1974). A schematic drawing of a four-circle diffractometer is shown in Fig. 4.7.1.

Since the control of the four-circle diffractometer is the precursor of that of most modern diffraction techniques, we shall describe here the geometrical details involved in the Eulerian cradle variant of the single-crystal diffractometer.

The instrument can be described as follows: three points (i) the center of the source of the radiation (S), (ii) the center of the crystal (C), and (iii) the center of the receiving slit of the detector (D) define a plane, which call the *diffraction plane*. The axis passing through the crystal and perpendicular to the diffraction plane is called the *principal axis* of the instrument. Its direction remains fixed throughout the experiment (perpendicular to the table on which the instrument is mounted), and hence the diffraction plane is horizontal. The detector is therefore constrained to rotate about the principal axis only. The angle SCD equals $180^\circ - 2\theta$, where 2θ is the angle between the incident and the diffracted beam. The diffraction vector corresponding to the Bragg angle θ is parallel to the bisector of the angle SCD . The other axes of rotation are:

- *The χ axis.* This is an axis passing through the crystal and lying in the diffraction plane. In a conventional diffractometer, this is the symmetry axis of a ring on whose internal cylindrical surface the device to which the crystal is rigidly attached can be displaced by a predetermined angle, called the χ angle. The center of the crystal must coincide with the center of the χ ring, throughout the experiment, and the plane of the χ ring is perpendicular to the diffraction plane.
- *The ϕ axis.* This is an axis about which the crystal, together with the device to which the crystal is rigidly attached, can be rotated through a predetermined angle, called the ϕ angle. The device carrying the crystal is called the goniometer head. During the rotation about the ϕ axis the center of the crystal must remain at the center of the χ ring and the orientation of the axis of rotation of the crystal within the plane of the ring is determined by the χ angle.
- *The Ω axis.* This axis passes through the crystal and through the plane of the χ ring, and is perpendicular to the diffraction plane. By definition, the Ω axis coincides with the principal axis of the instrument. Physically, however, there are two independent rotations associated with this axis: the Ω motor rotates the χ ring (with everything it carries) and does not affect the position of the detector, and the 2θ motor rotates the detector without affecting the orientation of the crystal with respect to the incident beam.
- *The ψ axis.* This is (usually) a virtual axis, the direction of which coincides with the direction of the diffraction vector. If the crystal is very small, or ground to a sphere, rotation of the crystal about the ψ axis will not cause appreciable fluctuations in the diffracted intensity corresponding to this vector. If, on the other hand, the crystal is strongly anisotropic (for example, if the crystal has the form of a platelet or a needle), the intensity of diffracted radiation will in general vary as the crystal is rotated about the ψ axis, because of varying absorption. The ψ rotation can be realized by a suitable combination of the angles χ , ϕ , and Ω .

In a diffraction experiment performed with the aid of a four-circle diffractometer, the diffraction vector is represented in terms of several sets of basis

vectors:

1. The conventional basis of the reciprocal lattice, the coordinates of the diffraction vector are simply the integers appearing in the Laue equations. This representation can be written as

$$\mathbf{h} = h\mathbf{a}^* + k\mathbf{b}^* + l\mathbf{c}^* \equiv \mathbf{H}^T \mathbf{A}^*, \quad (4.19)$$

where $\mathbf{H}^T = (h \ k \ l)$ and $\mathbf{A}^{*T} = (\mathbf{a}^* \ \mathbf{b}^* \ \mathbf{c}^*)$.

2. An orthonormal basis attached to the diffraction vector and the diffractometer. Such a basis is needed for the construction of the laboratory working system. We represent \mathbf{h} in this system as

$$\mathbf{h} = \mathbf{X}_D^T \mathbf{E}_D, \quad (4.20)$$

where $\mathbf{X}_D^T = (x_D^1 \ x_D^2 \ x_D^3)$ and $\mathbf{E}_D^T = (\mathbf{e}_{1D} \ \mathbf{e}_{2D} \ \mathbf{e}_{3D})$, and where the basis vectors \mathbf{e}_{jD} , $j = 1, 2, 3$, form a right-handed set of orthonormal (unit) vectors. These vectors are defined as follows:

- The vector \mathbf{e}_{2D} is parallel to the diffraction vector and therefore bisects the complementary angle $180^\circ - 2\theta$ between the incident and diffracted beams.
 - The vector \mathbf{e}_{1D} lies in the diffraction plane, is perpendicular to \mathbf{e}_{2D} and points to the source of radiation when $\theta = 0$.
 - The vector \mathbf{e}_{3D} coincides with the principal axis of the instrument and is directed so as to make the system of basis vectors right handed.
3. An orthonormal basis attached to the crystal and the diffractometer. This is a necessary mediator between the crystal system and the laboratory system. The diffraction vector is given in this system by

$$\mathbf{h} = \mathbf{X}_G^T \mathbf{E}_G, \quad (4.21)$$

where $\mathbf{X}_G^T = (x_G^1 \ x_G^2 \ x_G^3)$ and $\mathbf{E}_G^T = (\mathbf{e}_{1G} \ \mathbf{e}_{2G} \ \mathbf{e}_{3G})$, where the basis vectors \mathbf{e}_{jG} , $j = 1, 2, 3$, form a right-handed set of orthonormal (unit) vectors. The basis vectors in eqn (4.21) are defined so that the \mathbf{E}_G and \mathbf{E}_D sets of basis vectors coincide when $\chi = \phi = \Omega = 0$. Also, the unit vector \mathbf{e}_{3G} always coincides with the ϕ axis (the axis about which the goniometer head rotates).

For any values of the angles χ , ϕ , and Ω , the two orthonormal bases described above are related by a rotation matrix depending on these three angles, which correspond to a known triplet of Eulerian angles (see, for example, Goldstein, 1956; note, however, that the meaning of Goldstein's symbols is different from the present usage). This rotation matrix is obtained as a product of three rotation matrices about the corresponding axes. That is,

$$\mathbf{E}_G = \mathbf{F} \mathbf{E}_D, \quad (4.22)$$

where

$$\begin{aligned}
\mathbf{F} &= \mathbf{r}_\phi \mathbf{r}_\chi \mathbf{r}_\Omega \\
&= \begin{pmatrix} \cos \phi & \sin \phi & 0 \\ -\sin \phi & \cos \phi & 0 \\ 0 & 0 & 1 \end{pmatrix} \begin{pmatrix} 1 & 0 & 0 \\ 0 & \cos \chi & \sin \chi \\ 0 & -\sin \chi & \cos \chi \end{pmatrix} \begin{pmatrix} \cos \Omega & \sin \Omega & 0 \\ -\sin \Omega & \cos \Omega & 0 \\ 0 & 0 & 1 \end{pmatrix} \\
&= \begin{pmatrix} \cos \phi \cos \Omega - \sin \phi \sin \Omega \cos \chi & \cos \phi \sin \Omega - \sin \phi \cos \Omega \cos \chi & \sin \phi \sin \chi \\ -\sin \phi \cos \Omega - \cos \phi \sin \Omega \cos \chi & -\sin \phi \sin \Omega + \cos \phi \cos \Omega \cos \chi & \cos \phi \sin \chi \\ \sin \chi \sin \Omega & -\sin \chi \cos \Omega & \cos \chi \end{pmatrix}
\end{aligned} \tag{4.23}$$

Since, however,

$$\mathbf{h} = \mathbf{X}_G^T \mathbf{E}_G = \mathbf{X}_D^T \mathbf{E}_D = \mathbf{X}_D^T \mathbf{F}^{-1} \mathbf{F} \mathbf{E}_D$$

we must have

$$\mathbf{X}_G^T = \mathbf{X}_D^T \mathbf{F}^{-1}$$

or

$$\mathbf{X}_G = \mathbf{F} \mathbf{X}_D, \tag{4.24}$$

because a matrix of rigid rotation is orthogonal, and for such a matrix its inverse and transpose are identical.

4.7.2 The orientation matrix

It is very useful to define a matrix \mathbf{V} that satisfies the relation

$$\mathbf{A}^* = \mathbf{V} \mathbf{E}_G. \tag{4.25}$$

Each row of \mathbf{V} contains the Cartesian components of a basis vector of the reciprocal lattice, in the system linked to the crystal and diffractometer. If the orientation matrix is known, the unit cell dimensions can be obtained in a straightforward manner. It can be shown that

$$\mathbf{A}^* \cdot \mathbf{A}^{*T} = \mathbf{g}^{-1},$$

where \mathbf{g} is the matrix of the direct metric tensor (see Appendix B). Indeed

$$\begin{aligned}
\mathbf{A}^* \cdot \mathbf{A}^{*T} &= \mathbf{V} \mathbf{E}_G \cdot \mathbf{E}_G^T \mathbf{V}^T \\
&= \mathbf{V} \mathbf{V}^T
\end{aligned}$$

since $\mathbf{E}_G \cdot \mathbf{E}_G^T$ is a unit matrix. Therefore, the product $\mathbf{V} \mathbf{V}^T$ is indentially equal to the matrix of the metric tensor of the basis of the reciprocal lattice. By inverting this matrix, we obtain the matrix of the metric tensor of the basis of the direct lattice, and hence the direct unit cell parameters. The orientation matrix is of central importance in planning diffraction experiments by diffractometric methods as well as other methods.

4.7.3 Coordinates and angles

Recall that the diffraction vector \mathbf{h} is always parallel to the unit vector \mathbf{e}_{2D} of the orthonormal basis linked to \mathbf{h} and the diffractometer. For any reflection, we can therefore write $\mathbf{h} = |\mathbf{h}|\mathbf{e}_{2D}$, or

$$\mathbf{X}_D = \begin{pmatrix} 0 \\ |\mathbf{h}| \\ 0 \end{pmatrix}. \quad (4.26)$$

If we premultiply the right-hand side of eqn (4.26) by the rotation matrix \mathbf{F} given by eqn (4.23), we obtain the Cartesian coordinates of the diffraction vector in the system linked to the crystal and diffractometer,

$$\mathbf{X}_G = |\mathbf{h}| \begin{pmatrix} \cos \phi \sin \Omega + \sin \phi \cos \chi \cos \Omega \\ -\sin \phi \sin \Omega + \cos \phi \cos \chi \cos \Omega \\ -\sin \phi \cos \Omega \end{pmatrix}. \quad (4.27)$$

We now obtain, from eqns (4.19), (4.21) and (4.25),

$$\mathbf{H}^T \mathbf{A}^* = \mathbf{H}^T \mathbf{V} \mathbf{E}_G = \mathbf{X}_G^T \mathbf{E}_G,$$

from which it follows that

$$\mathbf{H}^T \mathbf{V} = \mathbf{X}_G^T. \quad (4.28)$$

If we know $\mathbf{H}^T = (h \ k \ l)$ and the orientation matrix \mathbf{V} , we can compute the components of \mathbf{X}_G and solve eqn (4.27) for the values of the angles χ, ϕ, Ω which are required in order to bring the crystal to an orientation at which the intensity of the reflection \mathbf{h} can be measured. Equations (4.27) and (4.28) are of value in programming a diffractometer to carry out intensity measurements for given ranges of reflection indices.

If, finally, we know the angular settings of a given reflection, for which the Cartesian coordinates of the corresponding diffraction vector can be computed from eqn (4.27) and the orientation matrix is also given, then the indices of this reflection are in principle found as

$$\mathbf{H} = (\mathbf{V}^T)^{-1} \mathbf{X}_G \quad (4.29)$$

Equation (4.29) is of importance for the indexing of reflections in the preliminary stages of the work.

It remains to show how the orientation matrix can be determined, or alternatively, how the Cartesian components of the basis vectors of the reciprocal lattice can be obtained. This can be usefully preceded by some comments on the experimental strategies employed.

4.7.4 Comments on the experiment

There are several methods of determining the orientation matrix, all of them requiring some preliminary experimental work. If some information about the

crystal is already available, for example from photographic work, this can be of value in the determination of the orientation matrix and the unit-cell parameters. It is, however, more common to “put the crystal on the diffractometer” in an arbitrary orientation and carry out an experiment. An important prerequisite is to bring the crystal to the center of the diffractometer system, at which all the axes of rotation intersect. This can be done manually by bringing the crystal to the center of the field of a properly aligned optical microscope. Once this is done, the computer-controlled operation of the diffractometer takes over. With the radiation on, the crystal is systematically scanned over the $\theta, \chi, \phi, \Omega$ space, until a significantly diffracting orientation is reached. Once it is there, the computer makes minor adjustments of the various axes until a maximum of a diffraction peak is obtained. The values of all four angles corresponding to the diffraction maximum are automatically recorded, and the magnitude of the diffraction vector is computed as $2 \sin \theta / \lambda$. The coordinates of the diffraction vector in the “G” Cartesian system can now be computed from eqn (4.27) and its direction is also defined. The automatic search for diffraction maxima continues until some 20 or so reflections have been recorded and the corresponding diffraction vectors defined. For better accuracy, the available reflections are checked together and recentered. An often useful alternative to the above systematic search is a rotation photograph taken on the diffractometer, on which the coordinates of some 20 or so reflections are measured and serve as an input to a program which locates the reflections in the $\theta, \chi, \phi, \Omega$ space. This procedure also involves a restricted search but is superior to a full systematic search, since the exposure of the crystal to radiation is significantly reduced. The next stage is an automatic indexing procedure. All the sums and differences of the available diffraction vectors are now sorted according to increasing magnitude, and the three shortest vectors which form intervector angles as close as possible to 90° are chosen as the basis vectors of the reciprocal lattice. Since their coordinates in the “G” system are available, a first approximation to the orientation matrix is immediately obtained, and so are the metric tensors of the reciprocal and direct bases, and the corresponding unit-cell dimensions. All the reflections which have so far been located are now indexed, and the unit-cell parameters are refined by a least-squares procedure, which also provides their standard deviations.

At this point the ranges of the indices hkl are specified and the collection of the intensity data collection is planned. There are several modes of scanning the diffraction space around each reflection, most of them being implemented on particular instruments. The process of data collection is usually automatic and its reliability can be monitored in a number of ways. A frequently applied way is to choose two or three strong reflections and remeasure their intensities at regular time intervals. The intensities of these so-called “standard” reflections give useful indications of the stability of the system (crystal + diffractometer). The actual measurement of the intensity of a reflection consists of (i) bringing the crystal and counter to an orientation corresponding to the maximum intensity of the reflection; (ii) performing a scan of the diffraction space around the

reflection according to the mode chosen, where the intensity is measured at each real or virtual step of the scan, thus creating an intensity profile; and (iii) integrating the intensity profile, including its background tails, and obtaining the net integrated intensity of the reflection along with the standard deviation of this intensity. Stage (iii) may range from a straightforward summation of intensity and background counts to more sophisticated profile analysis.

The results of this experiment, which are really the “raw material” for the determination of the crystal structure, are (i) the unit-cell dimensions and partial or complete information on the symmetry of the crystal (this subject will be discussed in the next chapter), and (ii) a number of records containing, for each reflection, its indices hkl , its net integrated intensity (or simply intensity) $I(hkl)$ and its standard deviation $\sigma_I(hkl)$. The actual planning of the experiment usually involves considerations of the accuracy which is aimed at and the number of structural parameters to be determined.

4.8 The Laue method

4.8.1 Principle of the method

The first diffraction pattern obtained by irradiating a stationary single crystal with a continuous spectrum of X-rays was observed by Friedrich, Knipping, and Laue (1912). Its interpretation was fully consistent with the existence of a periodic arrangement of material units within the crystal (Laue 1912), an idea which had been put forward in the eighteenth century and which gave rise to the theory of crystal symmetry—which dealt mainly with its microscopic aspects. It is most remarkable that the above experiment and all later diffraction experiments—even the most recent ones—bore out fully the theories of crystallographic lattices, point groups, and space groups, which were based mainly on macroscopic observations and on sound reasoning.

The technique based on the above experiment came to be known as the Laue method. The experimental arrangement is rather simple. The source of radiation is a continuous spectrum of X-rays, which fall directly on the crystal after passing through a “collimator”. The crystal is stationary, and the diffracted radiation is usually collected by a flat radiation-sensitive plate, perpendicular to the direction of the incident beam. In practice, the source can be a stationary-anode X-ray tube, a significantly more powerful rotating-anode X-ray tube, or, finally, a suitable range of X-rays selected from the spectrum of synchrotron radiation, the intensity of which is higher by several orders of magnitude than that emitted from laboratory X-ray tubes. The collector of diffracted radiation can be a photographic film or, as discussed above, an imaging plate, which is much more sensitive.

As we shall see in what follows, Laue patterns are not easily indexed, and were believed until recently to be of little or no use for structure determination. However, the most fruitful combination of a synchrotron source and an imaging-plate detector showed that a vast amount of information can be obtained in a

very short time, and thus stimulated a search for indexing algorithms. Applications of the Laue method to structure determination of protein crystals may be encountered in the recent literature (for example, Helliwell 1992).

A well-known property of a Laue pattern is that it allows one to determine the orientation of the crystal, say in terms of the coordinates of a reciprocal-lattice vector which is perpendicular to an irradiated crystal face. This has many application to metallurgy and materials science in general. The symmetry of the Laue pattern is very sensitive to deviations of the direction of the incident beam from the normal to the irradiated crystal face, and hence its use in orienting crystals. The symmetry of the weighted reciprocal lattice will be dealt with in the next chapter.

Let us now see what the origins of the Laue pattern are. Since a stationary crystal is irradiated here with polychromatic radiation, then instead of a single Ewald sphere, as in the case of monochromatic radiation, we have now a range of such spheres, the largest one corresponding to the shortest wavelength and the smallest to some arbitrarily chosen longest wavelength. Both spheres pass through the origin of the reciprocal lattice, and *any* reciprocal-lattice point lying within the large sphere and outside the small one corresponds to a possible reflection. This is how a stationary crystal can give rise to a large number of simultaneously produced reflections. We shall now show, expanding the derivation given by Rabinovich and Lourie (1987), how a Laue pattern can be computed or, perhaps, simulated. This procedure leads to the possibility of indexing the pattern.

4.8.2 Calculation of the Laue pattern

Let us assume that a polychromatic (“white”) X-ray beam is perpendicular to a circular flat plate that acts as a detector (a photographic film or an imaging plate), and passes through a stationary single crystal with known unit-cell dimensions. Let the crystal-to-plate distance be d centimeters, the radius of the plate be R_m centimeters, the X-ray tube operate at a high voltage of V volts, and the absolute maximum values of the diffraction indices be h_{\max} , k_{\max} and l_{\max} . Under these conditions, the shortest wavelength is given by

$$\lambda_{\min} = \frac{12\,398}{V} \text{ \AA},$$

the largest recordable Bragg angle is

$$\theta_{\max} = 0.5 \tan^{-1} \left(\frac{R_m}{d} \right),$$

and the largest magnitude of the diffraction vector is

$$|\mathbf{h}|_{\max} = \frac{2 \sin \theta_{\max}}{\lambda_{\min}}.$$

As indicated in Appendix B, a knowledge of the unit-cell dimensions enables us to obtain the matrix of the metric tensor of the direct lattice, with components

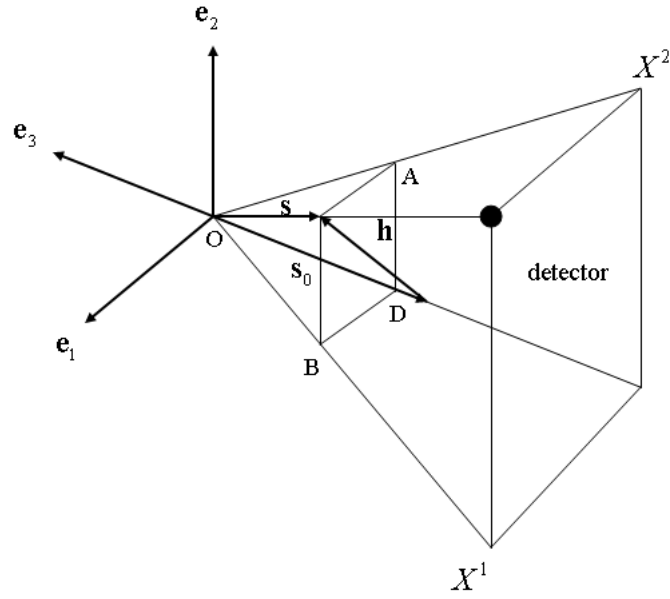


Fig. 4.13 *To the indexing of the Laue pattern.*

g_{ij} , and inversion of the latter matrix leads to the metric tensor of the reciprocal lattice, with components g^{ij} . This is of use in the calculation of the magnitude of the diffraction vector as

$$|\mathbf{h}| = \left(\sum_{i=1}^3 \sum_{j=1}^3 h_i h_j g^{ij} \right)^{1/2}, \quad (4.30)$$

where $-|h_{\max}| \leq h_1 \equiv h \leq h_{\max}$, $-|k_{\max}| \leq h_2 \equiv k \leq k_{\max}$, and $-|l_{\max}| \leq h_3 \equiv l \leq l_{\max}$ (see also Appendix B).

It is also convenient to define a Cartesian system in the diffraction device so that the unit vector \mathbf{e}_3 points towards the X-ray source (is antiparallel to \mathbf{s}_0), \mathbf{e}_1 is horizontal, \mathbf{e}_2 is vertical, and the three orthonormal basis vectors form a right-handed triad. (see Fig. 4.13). The diffraction vector in the reciprocal and Cartesian bases can then be written as

$$\mathbf{h} = \sum_{j=1}^3 h_j \mathbf{a}^j = \sum_{i=1}^3 q^i \mathbf{e}_i. \quad (4.31)$$

If we relate the basis vectors of the reciprocal lattice to the Cartesian basis by means of an orientation matrix, say \mathbf{D} , the diffraction vector can be written as

$$\mathbf{h} = \sum_{j=1}^3 h_j \sum_{i=1}^3 D^{ji} \mathbf{e}_i, \quad (4.32)$$

and the Cartesian components of the diffraction vector are therefore given by

$$q^i = \sum_{j=1}^3 h_j D^{ji}. \quad (4.33)$$

The components of the wavevectors \mathbf{s} and \mathbf{s}_0 are now

$$\mathbf{s}_0 : (0, 0, -1/\lambda) \quad (4.34)$$

and

$$\mathbf{s} = \mathbf{h} + \mathbf{s}_0 : (q^1\lambda, q^2\lambda, q^3\lambda - 1)/\lambda. \quad (4.35)$$

Let us now consider a plane in reciprocal space, perpendicular to the wavevector \mathbf{s}_0 and passing through the endpoint of \mathbf{s} (see Fig. 4.13). The distance of the plane from the center of the sphere corresponding to the current diffraction vector is the projection of \mathbf{s} onto the direction of \mathbf{s}_0 ,

$$OD = \mathbf{s} \cdot \frac{\mathbf{s}_0}{|\mathbf{s}_0|} = \frac{1 - q^3\lambda}{\lambda} = \frac{\cos(2\theta)}{\lambda}, \quad (4.36)$$

which readily leads to an expression for the wavelength corresponding to the current diffraction vector. Indeed,

$$q^3\lambda = 1 - \cos(2\theta) = 2\sin^2\theta$$

and

$$q^3 = \frac{2\sin\theta}{\lambda} \sin\theta = |\mathbf{h}| \sin\theta.$$

On the other hand, we always have $|\mathbf{h}| = (2\sin\theta)/\lambda$. It follows that

$$\lambda = \frac{2q^3}{|\mathbf{h}|^2}. \quad (4.37)$$

The other components of the wavevector \mathbf{s} are

$$AD = \mathbf{s} \cdot \mathbf{e}_1 = q^1 \text{ and } BD = \mathbf{s} \cdot \mathbf{e}_2 = q^2. \quad (4.38)$$

If the plane ABD is projected onto the flat detector, the coordinates of the diffraction spot, measured in centimeters from the center of the circular plate, can be obtained from the similar triangles shown in Fig. 4.13, as

$$X^1 = d \frac{AD}{OD} = d \frac{q^1\lambda}{1 - q^3\lambda} \quad (4.39)$$

and

$$X^2 = d \frac{BD}{OD} = d \frac{q^2\lambda}{1 - q^3\lambda}. \quad (4.40)$$

Given the orientation matrix \mathbf{D} , the coordinates of the diffraction spot can now be related to the diffraction indices $h_1 h_2 h_3$ for the wavelength given by eqn (4.37).

A possible practical realization of the above algorithm would be to mount a crystal on a four-circle diffractometer, obtain its orientation matrix and unit-cell dimensions, record the Laue pattern (either on the diffractometer or after transferring the crystal to a Laue device), and compare it with the pattern computed as indicated above.

4.9 Exercises for Chapter 4

1. The Laue equations can be written as

$$\mathbf{a}_1 \cdot \mathbf{h} = h_1, \quad \mathbf{a}_2 \cdot \mathbf{h} = h_2, \quad \mathbf{a}_3 \cdot \mathbf{h} = h_3$$

and the vector \mathbf{h} then becomes

$$\mathbf{h} = h_1 \mathbf{a}_1^* + h_2 \mathbf{a}_2^* + h_3 \mathbf{a}_3^*,$$

where $\mathbf{a}_1^* \mathbf{a}_2^* \mathbf{a}_3^*$ are basis vectors of the reciprocal lattice. However, the vector \mathbf{h} can also be referred to the direct basis vectors $\mathbf{a}_1 \mathbf{a}_2 \mathbf{a}_3$ as

$$\mathbf{h} = q_1 \mathbf{a}_1 + q_2 \mathbf{a}_2 + q_3 \mathbf{a}_3.$$

Find and interpret the transformation matrices \mathbf{P} and \mathbf{Q} relating the coordinates of \mathbf{h} in the above two representations in accordance with

$$h_i = \sum_{j=1}^3 Q_{ij} q_j \quad \text{and} \quad q_i = \sum_{j=1}^3 P_{ij} h_j.$$

2. A crystal was investigated by scientists I and II. Each of them assigned to it a different unit cell and the relation between the basis vectors they chose is:

$$\begin{aligned} \mathbf{a}_{II} &= \mathbf{a}_I - \mathbf{b}_I \\ \mathbf{b}_{II} &= \mathbf{a}_I + \mathbf{b}_I \\ \mathbf{c}_{II} &= \mathbf{c}_I \end{aligned}$$

What is the relation between the diffraction indices hkl that I and II assigned to the reflections they observed? Can this be generalized to any linear transformation of the basis vectors?

3. For a given crystal, consider the transformation

$$\mathbf{a}' = (\mathbf{b} + \mathbf{c})/2, \quad \mathbf{b}' = (\mathbf{c} + \mathbf{a})/2, \quad \mathbf{c}' = (\mathbf{a} + \mathbf{b})/2,$$

where \mathbf{abc} are the basis vectors of a Bravais lattice of type F . Find the relation between the diffraction indices $h'k'l'$ and hkl and hence the condition for possible reflections hkl from this crystal. Show that the unit cell based on the vectors \mathbf{a}' , \mathbf{b}' , and \mathbf{c}' is primitive.

(Note: The primed indices correspond to primed basis vectors, etc).

4. The volume of a primitive unit cell of a certain crystal is $V = 1564 \text{ \AA}^3$. What are the approximate total numbers of reflections which can be obtained from this crystal when it is irradiated with copper and molybdenum radiation?

(Assume that $\lambda(K\alpha_{av})$ is being used.)